

Characterization of self-repairing performance and thermodynamic study of the SiO₂-CaCO₃ supported graphene oxide in cement composites

Yi Zhang ^{a,*}, Dexin Hu ^a, Hailiang Wang ^a, Lei Cai ^a, Chen Niu ^a, Dongxu Li ^b

^a School of Materials Science and Engineering, Anhui University of Technology, Ma'anshan 243032, China

^b College of Materials Science and Engineering, Nanjing Tech University, Nanjing 210009, China

ARTICLE INFO

Keywords:

Graphene oxide, Self-repairing
Pozzolanic reaction
Nucleation effect
Hydration behavior

ABSTRACT

Nano-SiO₂ and CaCO₃ used as supporting material of GO (graphene oxide) and the SiO₂-CaCO₃-GO (SCG) was prepared, the self-repairing performance of the cement under the effect of the SCG were studied, the thermodynamic parameter of the cement were analyzed for the understanding of the SCG on the hydration behavior of the cement. The results showed that the mechanical properties of cement composites were improved, the cement composites had the compressive strength repair rate of up to 7.4 % as the addition of SCG, the surface cracks repair rate reached 100 %, which showed an obvious repairing effect than the control specimen. TG analysis showed that GO promoted the pozzolanic reaction between the nano-SiO₂ and Ca(OH)₂, SEM analysis showed that the interface between SCG and cement was gradually disappeared as the improved content of GO in SCG, indicating a good nucleation effect of GO in the cement hydration. ICP-AES test and the thermodynamic study showed that SCG continuously provided a greater dissolution driving force for the dissolution of calcium silicate minerals CS (C₃S/C₂S), results in the generation of more and denser C-S-H gel in the cement composites.

1. Introduction

Cement concrete is the most widely used building materials around the world, however, the high brittleness of the cement concrete causes it to be cracking during the long-term service, if micro-crack is not repaired in time and develop into macro-crack, it will cause structural damage and further loss of bearing capacity [1–4]. Therefore, improving the internal microstructure of cement concrete and timely detecting and repairing micro-crack is particularly important for extending the service life of cement concrete and enhancing its durability [5–7].

Graphene oxide (GO) is a derivative of graphene, it is obtained by chemically oxidizing of graphene and grafting a layer of oxygen-containing functional groups (-COOH, -CO, -O-, etc.) on the surface, the oxygen-containing functional groups reduce the van der Waals force between the GO sheet, endowing GO with great chemical activity, enabling it to combine with cement hydration products to form strong chemical bonds, thereby obtaining a stronger interfacial bonding ability [8–10]. These advantages make GO widely used in various cementitious composites for the enhancement of the mechanical properties [11–13].

Studies have shown that the nucleation site effect of GO could promote the progress of the cement hydration reaction, realize the

* Corresponding author.

E-mail address: zhy1987@ahut.edu.cn (Y. Zhang).

Table 1

Chemical composition of P·I 42.5 Standard Cement (wt%).

Composition	CaO	SiO ₂	Al ₂ O ₃	SO ₃	Fe ₂ O ₃	MgO	TiO ₂	P ₂ O ₅	K ₂ O	LOI
Cement	64.51	20.23	4.83	2.05	3.15	1.87	0.38	0.07	0.83	1.6

effect of connecting and filling the micro-crack of the cement composites [14–16]. Mishra et al. [17] revealed that the 28 d hydration degree of the cement increased by 8.3 % as the addition of GO. Peng et al. [18] found that GO could effectively refine the grain size of the hydration products, thereby forming a denser network structure of cement composites. Edwards et al. [19] demonstrated that the addition of GO at a low dosage of 0.005 % could effectively improve the pore structure, the total porosity and cumulative pore volume of cement reduced by more than 3.7 % and 12 %, respectively. Liu et al. [20] found that the stably dispersed GO provided sufficient nucleation site for the hydration product in the cement paste, significantly shortening induction period during the cement hydration process. The excellent nucleation site effect of GO could regulate the hydration of cement, optimize the structure and composition of the hydration products [21–23]. However, GO is extremely prone to complexation with Ca²⁺ in the alkaline environment of cement, resulting in the agglomeration of GO in the cement paste [24,25].

Due to the fact that the GO sheets can undergo coordination complexation with the internal Ca²⁺ ions, GO is highly prone to agglomeration in the cement hydration environment. The usage of GO with other nanomaterials is an effective way to avoid the aggregation of GO and display a better coupling enhance effect in the cement composites. Nano-SiO₂ in cement paste could promote the early hydration of C₃S and accelerate the hydration reaction rate of cement, the reaction nano-SiO₂ with Ca(OH)₂ and the generation of C-S-H gel could fill the pore in cement paste and make the structure more compact, improved the impermeability, frost resistance and chemical erosion resistance of cement concrete material [26,27]. Besides that, nano-SiO₂ also can enhance the cohesion of cement and reduce the generation of cracks, extend the service life of cement concrete [28,29]. Zhang et al. [30] studied the effect of water reducers on dispersion of nano-silica (NS) in cement solution, the results showed that the synergistic effects of 1.0 % polycarboxylate superplasticizers and 1 h of ultrasonication enhances the dispersion of NS aggregates, thereby promoting the hydration reaction of cement and refining the pore structure. Yassin et al. [31] investigate the effect of micro silica (MS) and nanosilica (MS) on the flexural behavior and mechanical properties of Self-Compacted High-Performance concrete (SCHPC) through the experiment and numerical method, the results showed that adding NS at a content of 4 % is more effective than replacing or adding MS for SCHPC mixture to increase the concrete compressive strength, splitting tensile strength, and flexural tensile strength. Huang et al. [32] investigated the impact of colloidal nano silica (CNS) on the freeze-thaw durability of concrete, the experimental results suggested that the incorporation of CNS increases the total air content of the sample while reducing the average void size.

Calcium carbonate (CaCO₃) powder is widely used as mineral admixtures to improve the durability and low carbon development of concrete. Xia et al. [33] investigated the volume stability of white cement concrete by synergy of CaCO₃ powder and blast furnace slag, the results manifested that the early shrinkage, dry shrinkage, creep and compressive strength were improved, and the volume stability of composite concrete was enhanced through the synergy effect. Saingam et al. [34] investigated the preparation of the self-compacting concrete where 25–70 % Ordinary Portland Cement (OPC) was replaced with fly ash and calcined CaCO₃, the improvement of workability and compressive strength clearly showed the prospect of a considerable reduction in cement consumption while maintaining structural integrity. As a kind of modified material, nano-CaCO₃ providing an effective way to improve the performance and prolong its service life in cement composite by virtue of its unique small-size effect and surface effect. The addition of nano-CaCO₃ could provide nucleation site and accelerate cement hydration, fill the capillary pores inside cement composites [4,35], play the role of optimize the structure of the interface transition zone, reduce pores, and enhance the bonding performance of the interface [36].

The self-repairing performance is of great significance for improving the durability and service life of cement concrete [37,38], studies on self-repairing properties of cement are mostly based on microcapsule method, microbial method and crystalline admixtures method [39–43]. In this study, to avoid the complexation effect of GO in cement solution, SiO₂-CaCO₃-GO (SCG) was prepared by a simple blending method in which nano-SiO₂ and CaCO₃ were used as supporting materials, the influence of SCG on the self-repairing performance and hydration behavior of cement composites were investigated.

2. Experiment

2.1. Materials

Nano-SiO₂, with a specific surface area of 200 m²/g, Macklin Biochemical Technology Co., Ltd. CaCO₃, analytical purity, Sino-pharm Chemical Reagent Co., Ltd. Graphene oxide (GO), with a concentration of 10 mg/L, Soochow Tanfeng Technology Co., Ltd. P-I 42.5 standard cement, China United Cement Co., Ltd, complied with Chinese National Standard GB175–2007, the chemical composition of cement was shown in Table 1. Standard sand, Xiamen ISO Standard Sand Co., Ltd.

2.2. Preparation of SiO₂-CaCO₃-GO

SiO₂-CaCO₃-GO (SCG) particle was prepared by a simple blending method, in which SCG-A refers to the mass proportion of mSiO₂:mCaCO₃:mGO as 1:1:0.5, SCG-B refers to the mass proportion of mSiO₂:mCaCO₃:mGO as 1:1:1. XRD pattern of nano-SiO₂, CaCO₃ and

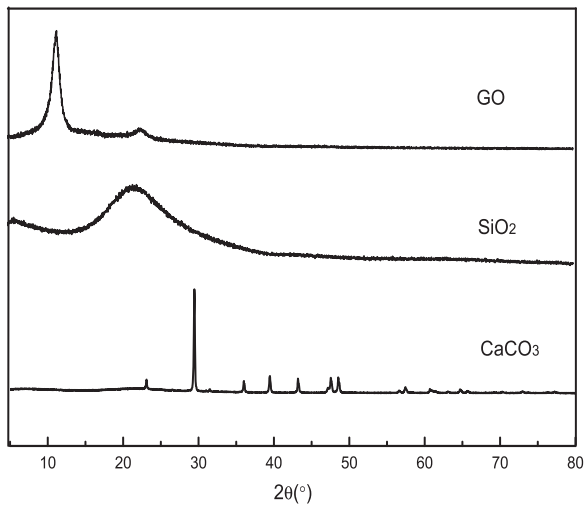


Fig. 1. XRD patterns of GO, nano-SiO₂ and CaCO₃.

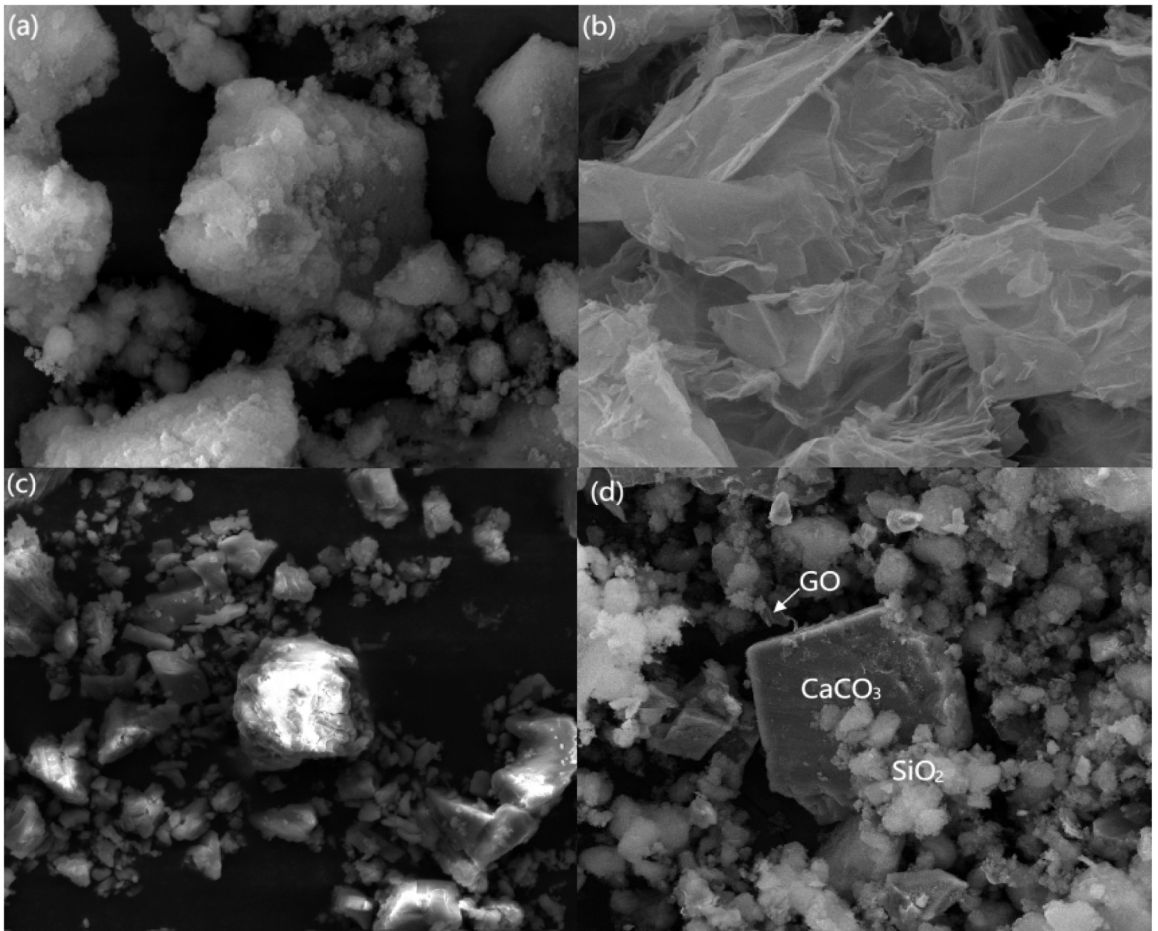


Fig. 2. SEM of SiO₂, GO, CaCO₃ and SCG-B: (a) SiO₂; (b) GO; (c) CaCO₃; (d) SCG-B.

GO is shown in Fig. 1, as can be seen from Fig. 1, $2\theta = 10.98^\circ$ corresponded to the diffraction peak of (001) plane of GO. Nano-SiO₂ was an amorphous state with a broad diffraction peak appeared around $2\theta = 22.06^\circ$. The diffraction characteristic peak of CaCO₃ was appeared at 20 of 29.4° , 36.02° , 39.46° , 43.18° , 47.48° , and 48.52° , corresponding to the (104), (110), (113), (202), (018), (118) of the

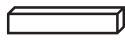
Table 2

Mix proportion of cement mortar/g.

Specimen	Cement	Sand	Water	SCG-A	SCG-B
Control	450	1350	225	—	—
SCG-A-1	450	1350	225	4.5	—
SCG-A-2	450	1350	225	9	—
SCG-A-3	450	1350	225	18	—
SCG-B-1	450	1350	225	—	4.5
SCG-B-2	450	1350	225	—	9
SCG-B-3	450	1350	225	—	18

Table 3

Size and number of specimens for each test.

Shape	Size	Number	Test performed
	40 × 40 × 160 mm	3	Mechanical performance test
	40 × 40 × 160 mm	2	Compressive strength repair rate
	Φ100mm × 50 mm	7	Surface crack repair rate

calcite, respectively.

SEM image of nano-SiO₂, GO, CaCO₃ and SCG-B is shown in Fig. 2, it can be seen that the GO was nanosheet structure within the size rang about 10–50 μm, the surface of GO was not flat that presented wrinkled and folded surface, the thickness of GO was about 1–5 nm. As can be seen from Fig. 2, GO, CaCO₃ and SiO₂ were well mixed, in which CaCO₃ and SiO₂ acted as dispersing role, enabling GO to be better dispersed in the cement matrix.

2.3. Preparation and mechanical performance test of cement mortar

The preparation and the mechanical performance test of the cement mortar was carried following the Chinese Standard of GB/T 17671–2021, the mixed proportion is shown in Table 2.

2.4. Self-repairing performance

2.4.1. Compressive strength repair rate

For the self-repairing test of the compressive strength, firstly, the failure compressive strength of the specimens at 28 d were recorded, then the pre-loading test was conducted on other specimens with 80 % of the failure load, the post-repair compressive strength of the specimen was tested at 2 h and 7 d stand curing [41], the compressive strength repair rate was calculated with Eq. (1).

$$\alpha = \frac{f_r - f_i}{f_i} \times 100\% \quad (1)$$

Where: α is the compressive strength repair rate, f_r is the post-repair compressive strength, f_i is the initial compressive strength of the specimens with 100% failed load.

2.4.2. Surface crack repair rate

For surface crack repair test, cylindrical specimen with the size of Φ100 mm × 50 mm was prepared and splitted at 28 d. The surface crack repair test at the specified curing age (0 d, 1 d, 3 d, 5 d, 7 d, 14 d, 28 d) was measured by image processing method using the software Image-pro Plus. The surface crack repair rate was calculated according to Eq. (2). In each mortar matrix, two types of specimens were made that following the molds as summarized in Table 3.

$$\gamma = \frac{S_i - S_t}{S_i} \times 100\% \quad (2)$$

Where: γ is the surface area crack repair rate, S_i is the initial crack area, S_t is the crack area at the different curing age.

2.5. Microscopic performance characterization

Powder XRD pattern was recorded using a Bruker AXS D8 diffractometer with a Cu target (K α radiation, $\lambda=1.54056 \text{ \AA}$), the scanning range is 5–80° (2 θ) and the scanning rate is 5°/min. The microscopic morphology of the specimen was characterized using a NANO SEM430 FESEM, with an accelerating voltage of 15 kV. The thermogravimetric analysis was measured by a DTG-60H

Table 4
Thermodynamic fitting parameters for calculating activity coefficient.

Ion species	Deby-Hückel \bar{a}	Deby-Hückel $b\gamma$
Ca^{2+}	5	0.165
H^+	9	0
SO_4^{2-}	5	-0.04

Table 5
Thermodynamic parameters used to calculate solubility and saturation index (25 °C).

Ion species	Reaction process	$\log K_{\text{sp}}$
OH^-	$\text{H}_2\text{O} - \text{H}^+$	-14.00
CaOH^+	$\text{Ca}^{2+} + \text{OH}^-$	1.18
C_3S	$3\text{Ca}^{2+} + \text{H}_3\text{SiO}_4^0 + 6\text{OH}^- - 5\text{H}_2\text{O}$	-24.11
$\text{Ca}(\text{OH})_2$	$\text{Ca}^{2+} + 2\text{OH}^-$	-5.18
C_2S	$2\text{Ca}^{2+} + \text{H}_3\text{SiO}_4^- + \text{H}^+ + 4\text{OH}^- - 4\text{H}_2\text{O}$	39.18
H_3SiO_4^0	$\text{H}_4\text{SiO}_4^- - \text{H}^+$	-9.83

thermogravimetric analyzer, under a nitrogen atmosphere, specimen was heated from room temperature to 900 °C at a heating rate of 10 °C/min. The element concentrations in different hydration stages in the cement solution was tested by an inductively coupled plasma atomic emission spectrometer (ICP-AES, ICPS-7510 PLUS), sample was dissolved in HNO_3 and the pH was adjusted to 2–3 with ultra pure water, and the clear liquid was taken out using a vacuum sand core filtration device.

2.6. Thermodynamic calculation

The activity of a single ion a_i is defined as its molar concentration (m_i) multiplied by the activity coefficient (γ_i), which expressed by Eq. (3). The commonly used formula for calculating the ion activity in the cement system solution are Davies (Eq. (4)) and the Deby-Hückel extended formula (Eq. (5)), I_m is the effective molar ionic strength, and its calculation method is shown in Eq. (6).

$$a_i = m_i \gamma_i \quad (3)$$

$$\log \gamma_i = -A_\gamma Z_i^2 \left(\frac{\sqrt{I_m}}{1 + \sqrt{I_m}} - 0.3I_m \right) \quad (4)$$

$$\log \gamma_i = \frac{-A_\gamma Z_i^2 \sqrt{I_m}}{1 + \hat{a} B_\gamma \sqrt{I_m}} + b_\gamma I_m \quad (5)$$

$$I_m = \frac{1}{2} \sum m_i Z_i^2 \quad (6)$$

Where a_i is the activity of ion i, m_i is the molar concentration of ion i; γ_i -the activity coefficient of ion i, Z_i is the charge number of ion i; A_γ and B_γ is the constants related to temperature and pressure, under the conditions of 25 °C and standard atmospheric pressure, their values are 0.51 and 0.33, respectively; \hat{a} and b_γ is independent parameters fitted for each ion with pure salt solution. \hat{a} and b_γ of some ions in the cement solution is given in Table 4.

The saturation index (SI) is based on thermodynamics can be calculated by Eq. (7), which is used to evaluate the dissolution, precipitation or equilibrium state of the solid phase in the solid-liquid phase system. When $SI < 0$, it indicates that the concentration of the solid phase in the solution is not saturated, and the solid phase tends to dissolve[44].

$$SI = \lg \left(\frac{IAP}{K_{\text{sp}}} \right) \quad (7)$$

Table 5 gives the reactions used in some thermodynamic calculations and the K_{sp} values of some ions/compounds [45]. It can be seen that in the calculation of the SI , the calculation of the ion activity product (IAP) is involved. The IAP is an indicator of the unsaturation of the compound, and it is closely related to the concentration of each element in the compound and the pH value of the cement solution, the calculation of the IAP of C_3S is shown in Eq. (8).

$$IAP_{\text{C}_3\text{S}} = (\text{Ca}^{2+})^3 (\text{H}_3\text{SiO}_4^-)(\text{OH}^-)^6 \quad (8)$$

Where SI is the saturation index, IAP is the ion activity product, K_{sp} is the solubility product.

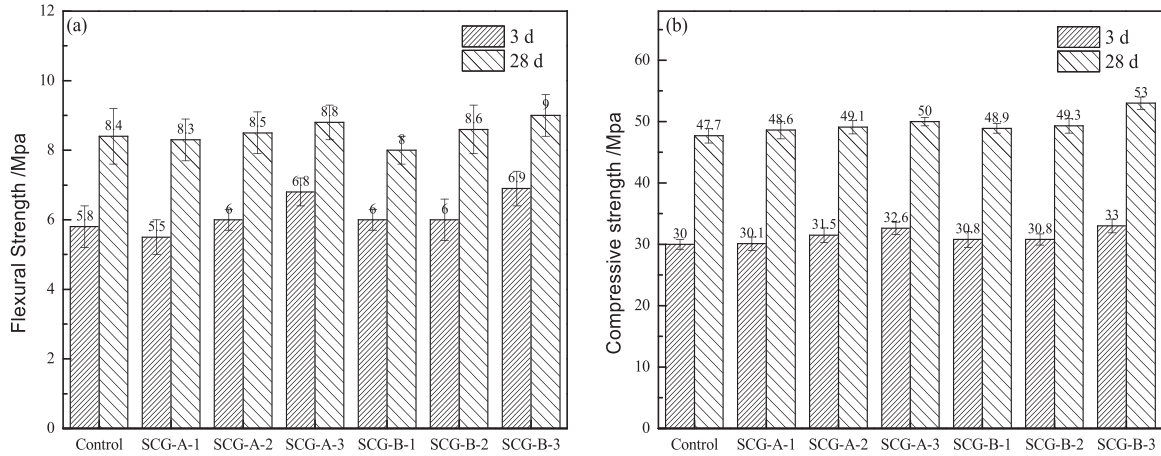


Fig. 3. Mechanical performance of the specimens: (a) Flexural strength; (b) Compressive strength.

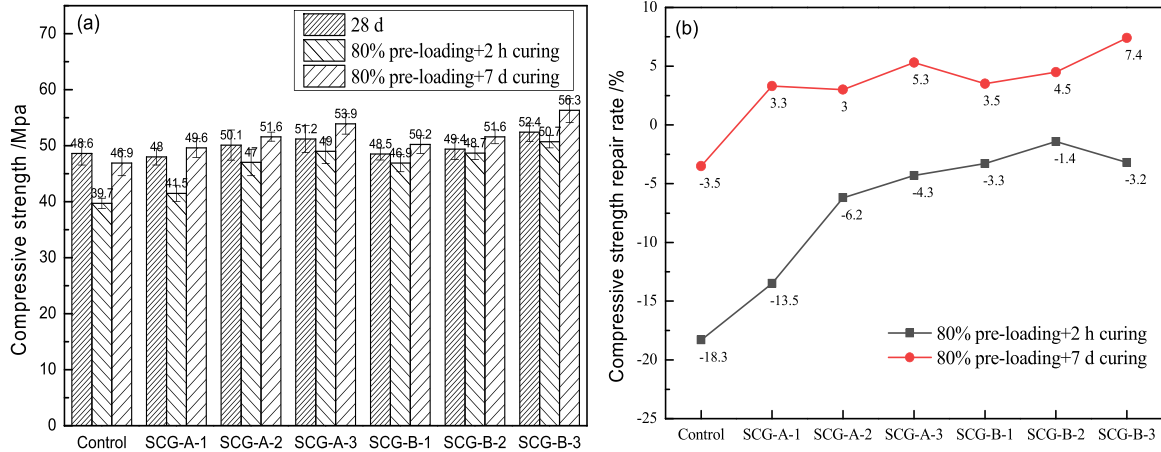


Fig. 4. The post-repaired compressive strength and compressive strength repair rate after 2 h and 7 d repairing: (a) post-repaired compressive strength; (b) compressive strength repair rate.

3. Results and discussion

3.1. Mechanical performance

The flexural and compressive strength of the cement mortar at 3 d and 28 d is shown in Fig. 3. It can be seen from Fig. 3(a) that the flexural strength of cement was gradually increased as the increase amount of SCG. With the increase amount of SCG, the flexural strengths of the SCG-B-3 specimen at 3 d and 28 d increased by 19 % and 7.1 % compared with the control. As can be seen from Fig. 3 (b), the compressive strength was increased as the incorporation of SCG, the compressive strengths of SCG-A-3 at 3 d and 28 d increased by 8.7 % and 4.8 %; respectively, and the increased rate of SCG-B-3 were 10 % and 11.1 %, it is showed that the improved content of GO in SCG improved the mechanical strength of the cement mortar.

3.2. Compressive strength repair rate

The compressive strength of the specimen after 2 h and 7 d post-repairing is shown in Fig. 4. The compressive strength of the control at 2 h and 7 d was decreased to 39.7 MPa and 46.9 MPa, respectively. Compared with the initial 48 MPa, the compressive strength at 7 d increased to 49.6 MPa with 1 % SCG-A-1. As shown in Fig. 4, the compressive strength repair rate at 2 h and 7 d of the SCG-A-3 composites were -4.3 % and 5.3 %, respectively. The compressive strength repair rate at 2 h and 7 d of the SCG-B were higher than the SCG-A composites, the compressive strength repair rate at 2 h and 7 d of SCG-B-3 were -3.2 % and 7.4 %, respectively. The addition of SCG promoted the mechanical strength repairing and with the increased content of GO, the compressive strength repair rate of the SCG composites further improved.

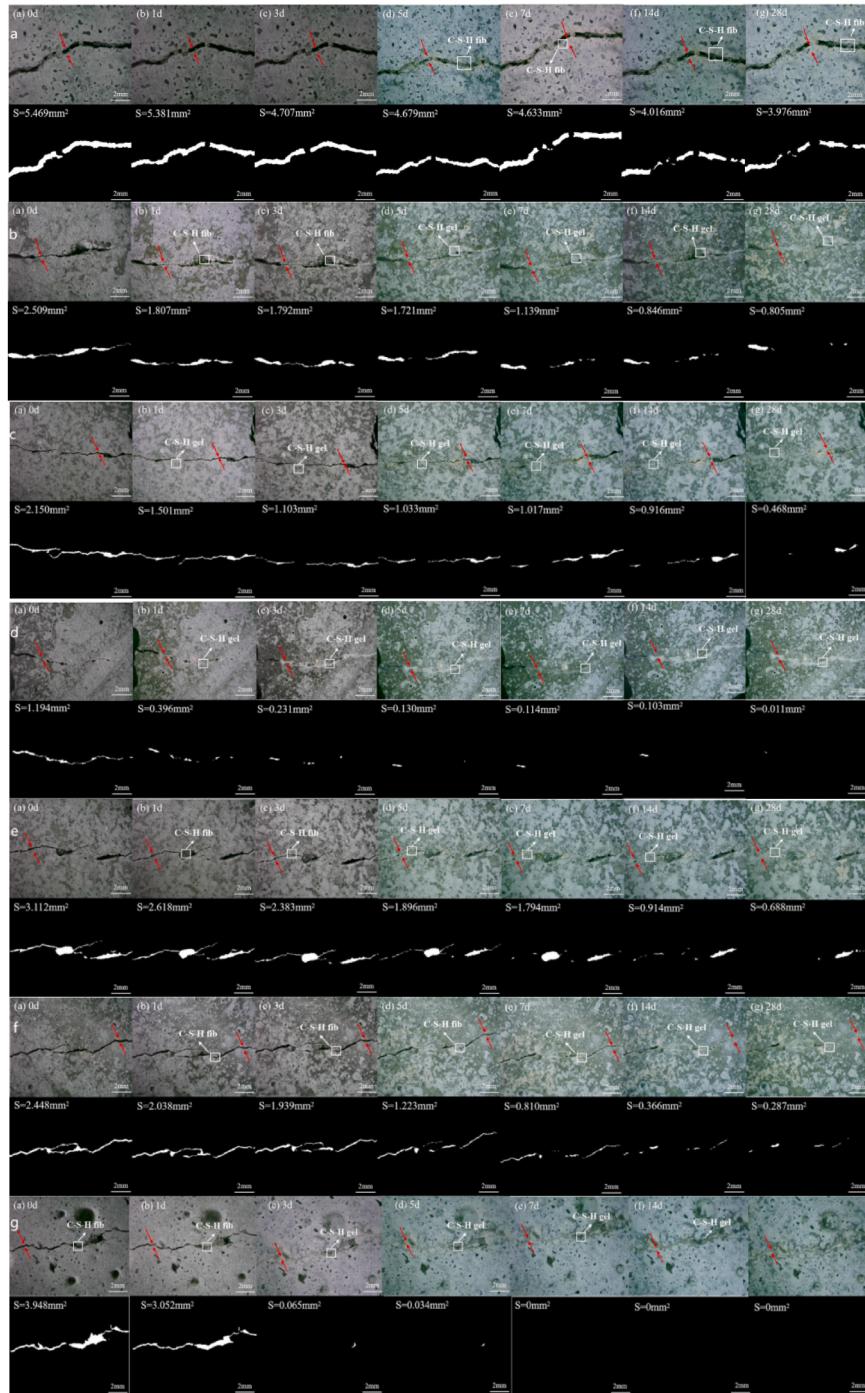


Fig. 5. Crack repair photograph of the specimens at different curing age: a. Control; b. SCG-A-1; c. SCG-A-2; d. SCG-A-3; e. SCG-B-1; f. SCG-B-2; g. SCG-B-3.

3.3. Surface crack repair rate

Taken by the optical microscope and analyzed by the Image-Pro Plus, photograph at different curing age (0 d, 1 d, 3 d, 5 d, 7 d, 14 d, 28 d) are shown in Fig. 5. It can be seen from Fig. 5(a) that the control specimen was partly repaired where the loose structure C-S-H fiber appeared on the crack surface, the repair area at 28 d decreased to 3.976 mm² from the initial 5.469 mm², the surface crack repair rate is about 27.3 %.

As shown in Fig. 5(b)~d, with the increased amount of SCG, the surface crack was well filled by the dense structure of C-S-H gel

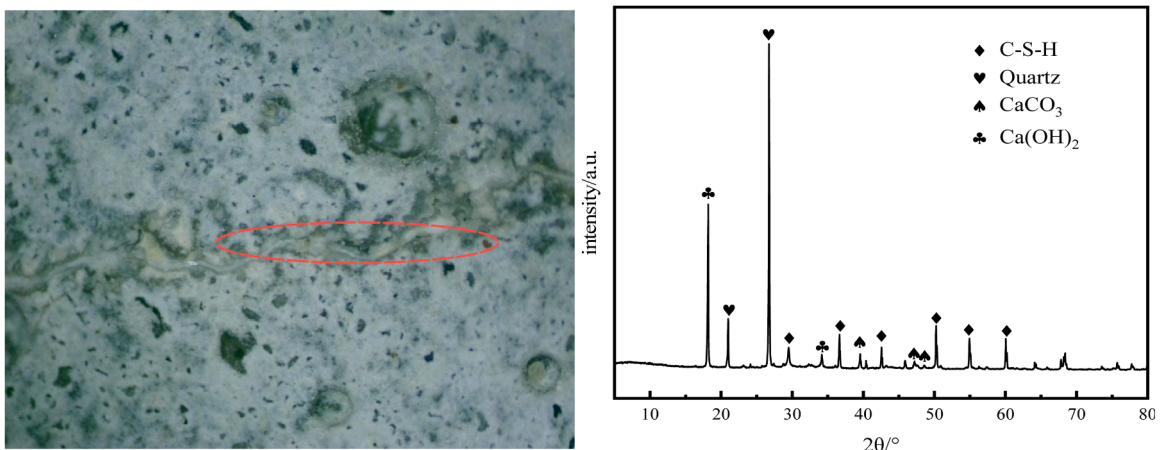


Fig. 6. Crack repairing of SCG-B-3 specimens and XRD spectrum of crack repair product.

after 28 d repairing, the surface crack repair rate of SCG-A-1, SCG-A-2, and SCG-A-3 were 67.9 %, 78.2 % and 99.1 %, respectively, it seemed that the appearance time of C-S-H gel in SCG-A-2 and SCG-A-3 was advanced to 3 d compared with 5 d of SCG-A-1; as shown in Fig. 5(e)~g, as the increased amount of SCG-B, the formation of the C-S-H gel of SCG-B-3 was advanced to 3 d compared with 5 d of SCG-B-1 and SCG-B-2, the surface crack repair rate of SCG-B-1, SCG-B-2, and SCG-B-3 composites were 78.5 %, 97.9 % and 100 %, respectively, the surface crack was completely repaired at 7 d for the SCG-B-3 composites. Compared with the control, the surface crack repair rate of the SCG was obviously increased, as the increase in the proportion of GO in SCG-B, denser C-S-H gel was produced in the SCG-B composite, when the SCG content reached 2 % and 4 %, the SCG-B composite showed a higher surface crack repair efficiency, the more GO incorporation in SCG, the more obvious the crack self-healing effect and the higher surface crack repair rate were seen from the cement matrix.

The self-repairing product in the crack of the SCG-B-3 specimen was taken out with a small knife, XRD spectrum of the self-repairing product was tested to study the composition of the repairing product, as shown in Fig. 6. As can be seen from Fig. 6, the crack repair product was mainly the C-S-H, $\text{Ca}(\text{OH})_2$, and CaCO_3 ; since the crack was exposed outside from the air and CO_2 was adsorbed, CaCO_3 precipitate was formed, and the quartz sand mainly came from the standard sand in the mortar.

3.4. XRD analysis of hydration products

XRD patterns of the hydration products of each specimen at 3 d and 28 d are shown in Fig. 7(a)–(g). The main components of the cement were $\text{Ca}(\text{OH})_2$, C-S-H, unhydrated C_2S , C_3S , it can be seen that for the control, SCG-A-1 and SCG-B-1 specimens, the diffraction peak intensity of $\text{Ca}(\text{OH})_2$ was obviously increased compared with 3 d. For the specimens of SCG-A-2 to SCG-B-3, the diffraction peak intensity of $\text{Ca}(\text{OH})_2$ at 28 d was not increased significantly compared with 3 d, with the increase amount of SCG, sufficient SiO_2 was supplied, GO in SCG provided sufficient nucleation site, more $\text{Ca}(\text{OH})_2$ was consumed in the pozzolanic reaction with SiO_2 , and more C-S-H gel was generated in the SCG cement composites.

3.5. Thermogravimetric analysis

Thermogravimetric (TG) curves of the specimens are shown in Fig. 8, three endothermic peaks can be clearly seen on the DTG curves, the first peak around 100 °C was the endothermic peak generated by water loss or decomposition of C-S-H and ettringite; the second peak around 400–480 °C was the endothermic peak of decomposition of $\text{Ca}(\text{OH})_2$; the third absorption peak between 600 and 700 °C was the decomposition of CaCO_3 . Since the weight loss recorded in the TG curve is the evaporation of water after high temperature heating of $\text{Ca}(\text{OH})_2$, the content of $\text{Ca}(\text{OH})_2$ in the composites can be obtained by Eq. (9).

$$m_{\text{ca}(\text{OH})_2} = \frac{M_{\text{ca}(\text{OH})_2} \times m_{\text{H}_2\text{O}}}{M_{\text{H}_2\text{O}}} \quad (9)$$

Where: $m_{\text{ca}(\text{OH})_2}$ is $\text{Ca}(\text{OH})_2$ content in the cement composites(%), $M_{\text{ca}(\text{OH})_2}$ is the molecular weight of $\text{Ca}(\text{OH})_2$ which is 74, $M_{\text{H}_2\text{O}}$ is the molecular weight of H_2O which is 18, $m_{\text{H}_2\text{O}}$ is the amount of the weight loss during 400–480 °C.

The $\text{Ca}(\text{OH})_2$ content calculated from Eq. (9) is shown in Fig. 9. Compared with the control, the $\text{Ca}(\text{OH})_2$ content in the SCG composite decreased at 3 d, promoted by the nucleation site effect of GO, nano- SiO_2 in SCG continuously reacted with $\text{Ca}(\text{OH})_2$ and more C-S-H gel was produced. Compared with the control specimen at 28 d, the content of $\text{Ca}(\text{OH})_2$ in the SCG-A-3 and SCG-B-3 composite decreased by 20.7 % and 22.7 %, respectively. The increase of GO in SCG-B could provide more sufficient nucleation substrates for the continuous hydration of CS ($\text{C}_2\text{S}/\text{C}_3\text{S}$) at the process of hydration stage, and the pozzolanic effect of SiO_2 in SCG was also accelerated, which resulted in the production of more C-S-H gel, so that the microcrack of cement could be better repaired under

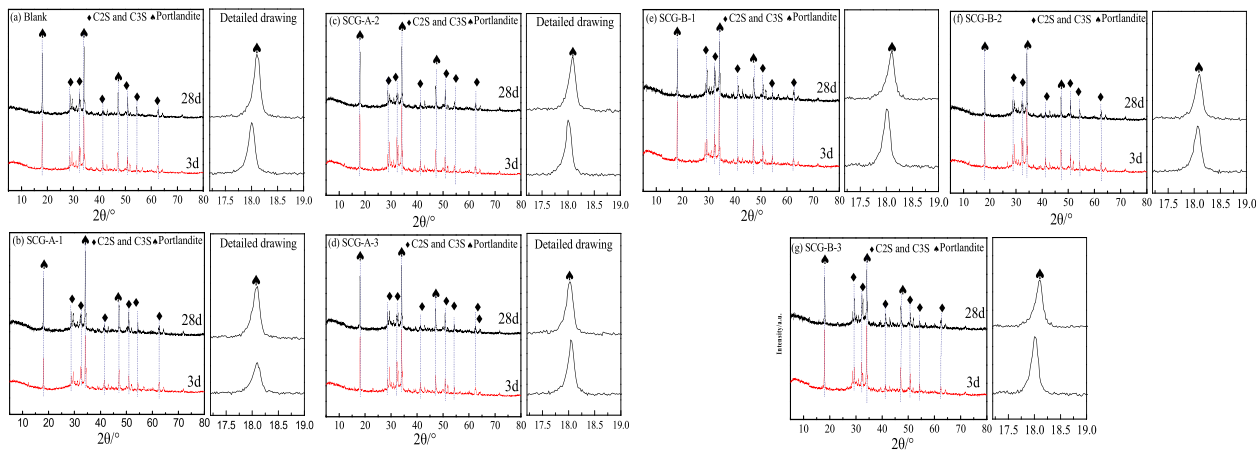


Fig. 7. XRD spectra of hydration products of each specimen at 3d and 28d: (a) control; (b) SCG-A-1; (c) SCG-A-2; (d) SCG-A-3; (e) SCG-B-1; (f) SCG-B-2; (g) SCG-B-3.

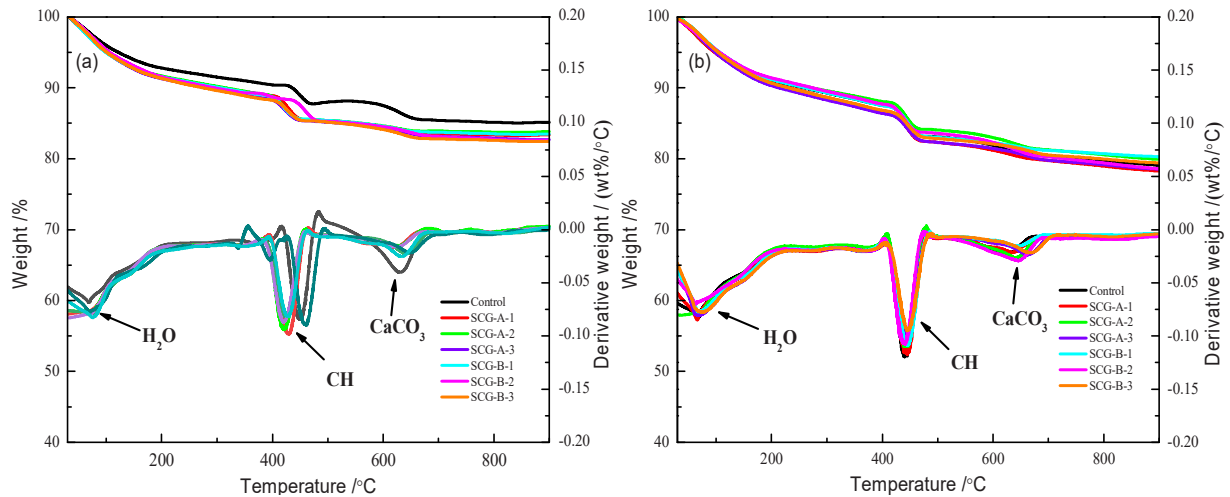


Fig. 8. TG-DTG curves of cement pastes of each specimen: (a) 3 d; (b) 28 d.

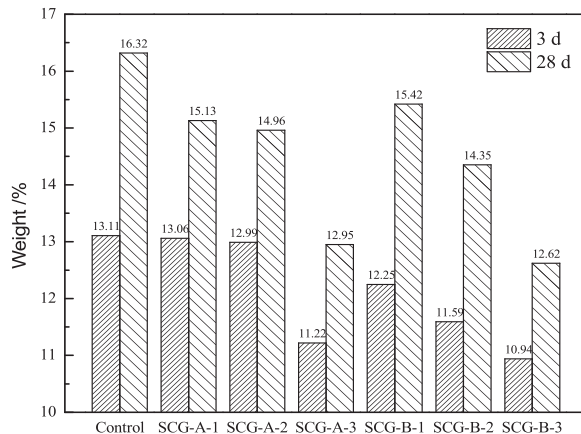


Fig. 9. Ca(OH)₂ content of the specimens at 3 d and 28 d.

the effect of the SCG.

3.6. SEM analysis

The microscopic morphology of cement at 3 d are shown in Fig. 10. As can be seen from Fig. 10(a), the microstructure of the control specimen was relatively loose, hexagonal plate Ca(OH)₂, C-S-H gel and the needle-like ettringite were generated and interspersed with each other. From Fig. 10(b)~(d), with the addition of SCG-A, an obvious interfacial transition zone (ITZ) appeared between the cement and SCG; as can be seen from Fig. 10(e)~(g), compared with SCG-A, due to the increased proportion of GO, more hydration product adsorbed on the surface of the SCG-B, the interface between SCG-B and cement gradually disappeared, the integrated degree of the SCG-B with the cement was further improved.

The microscopic morphology of the cement at 28 d are shown in Fig. 11. As can be seen from Fig. 11(a), as the advanced of the hydration process, C-S-H gel, ettringite were clearly seen in the control, the hydration products intersected and overlapped with each other, and a more compact structure of the cement was formed. From Fig. 11(b)~(d), more hydration products appeared and the interface between SCG-A and cement matrix was fully filled. Compared with SCG-A composites, as shown in Fig. 11(e)~(g), with the increase of GO content, the interface of the SCG-B-3 was basically disappeared, the pozzolanic reaction of nano-SiO₂ enable the filling of the interface in the cement composite.

3.7. Effect of SCG on element concentration of cement dissolution

The variation trend of the concentrations of Ca and Na elements in the control and SCG-B-3 over time is shown in Fig. 12. The concentration of Ca element (C_{ca}) in the pore solution of control was 43.186 mmol/L at 1 h, while the C_{ca} in the SCG solution was

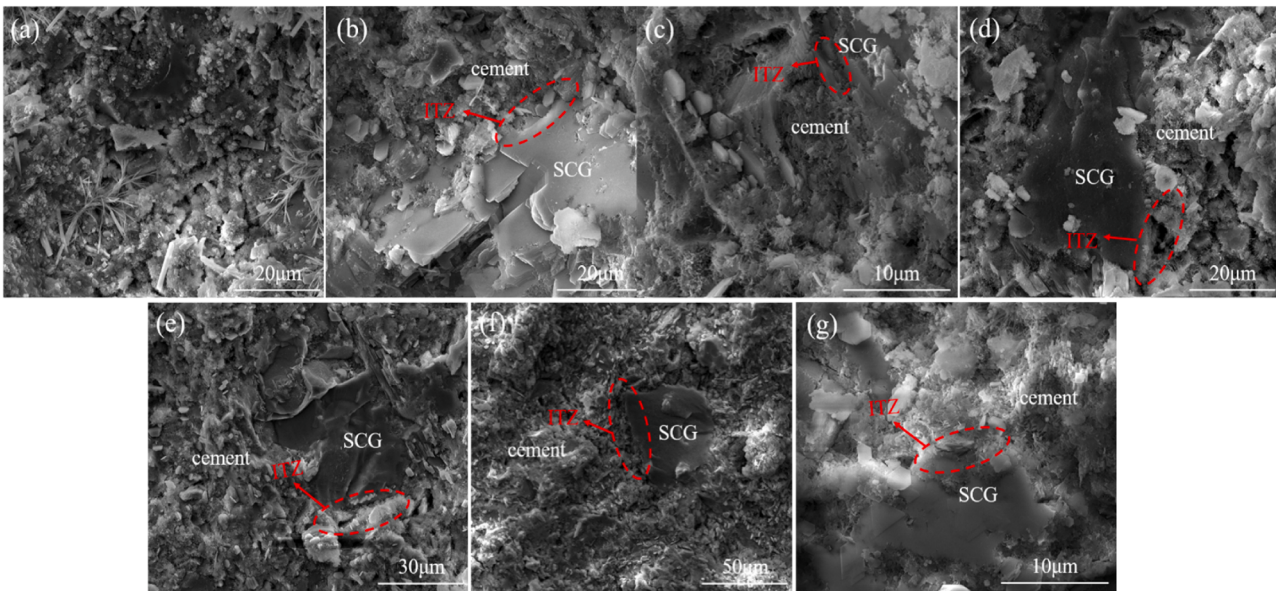


Fig. 10. Microscopic morphology of hydration products of the specimens at 3 d: (a) Control; (b) SCG-A-1; (c) SCG-A-2; (d) SCG-A-3; (e) SCG-B-1; (f) SCG-B-2; (g) SCG-B-3.

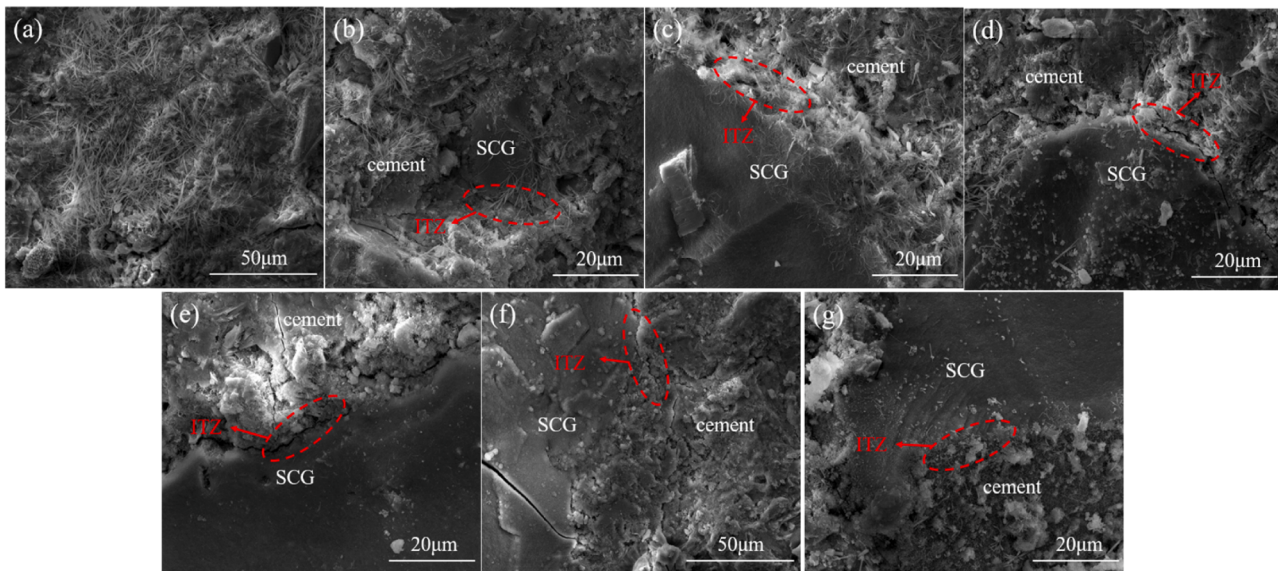


Fig. 11. Microscopic morphology of hydration products of the specimens at 28 d: (a) Control; (b) SCG-A-1; (c) SCG-A-2; (d) SCG-A-3; (e) SCG-B-1; (f) SCG-B-2; (g) SCG-B-3.

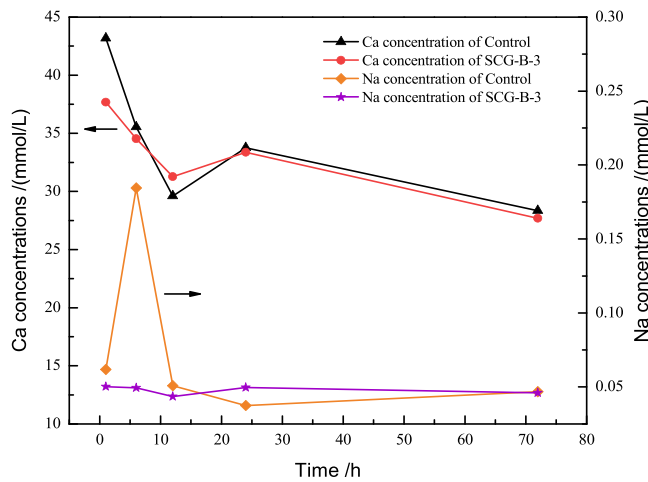


Fig. 12. Ion concentrations of Ca and Na in the control and SCG-B-3 cement solution.

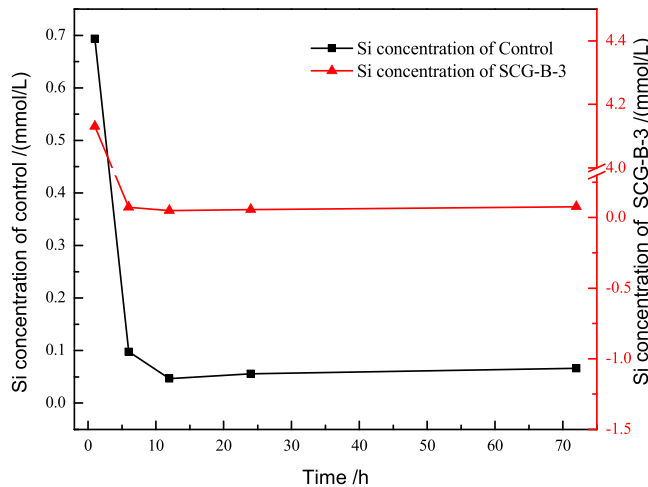


Fig. 13. Ion concentration of Si in the control and SCG-B-3 cement solution.

37.673 mmol/L, which was 12.77 % lower than that of the control. As the GO in the SCG adsorbed Ca^{2+} , the C_{ca} in the control was higher than that of the SCG until 6 h, resulted in a decrease in C_{ca} of the SCG cement solution. When the cement hydration proceeded to 12 h, the C_{ca} in the SCG exceeded the control, the adsorption of GO lead to a decrease in C_{ca} and simultaneously promoted the dissolution of calcium silicate minerals CS ($\text{C}_3\text{S}/\text{C}_2\text{S}$), supplementing a certain amount of Ca^{2+} to the solution, the C_{ca} in the SCG group was higher than that of the control. Starting from 24 h, as the continuously dissolving of CS, C_{ca} in the control was higher than that of the SCG again. Due to the excellent nucleation site effect of GO, the rate of precipitation of hydration products was greater than that of the control, lead to a faster consumption rate of Ca^{2+} in the SCG composites.

For the Na element, the existing form in the cement solution is Na^+ , the concentration of Na^+ (C_{Na}) in the control is higher than that of SCG between 1 and 12 h, just like the adsorption of Ca^{2+} , negatively charged GO would also adsorb Na^+ , resulted in a lower C_{Na} in the SCG composite. However, the C_{Na} concentration in the SCG was higher than control at 24 h, then gradually declined, the C_{Na} in the SCG was lower than the control again at 72 h, this also indicated that GO could promote the dissolution of CS in cement during the hydration process, thereby leading to a increase in the Na^+ concentration.

The trend of the Si concentration in the cement solutions of the control and SCG-B-3 over time is shown in Fig. 13. It can be seen from Fig. 9 that in the early stage of hydration, as a certain amount of Si included in the SCG, the Si concentration in SCG was much higher than that of the control specimen, the Si concentration of the control at 1 h was 0.69 mmol/L, while the Si concentration of the SCG-B-3 was 4.13 mmol/L. With the progress of cement hydration, Si concentration in SCG at 6 h began to be lower than that of the control, the Si concentration of the control was 0.10 mmol/L, while the Si concentration of the SCG-B-3 was 0.07 mmol/L, which indicated that SCG fully participated in the cement hydration and large amount of Si was consumed, resulted in a sharp decreased of Si concentration in the solution.

As the hydration reaction proceeded to 12 h, the Si concentration in the SCG began to be higher than that of the control, due to the

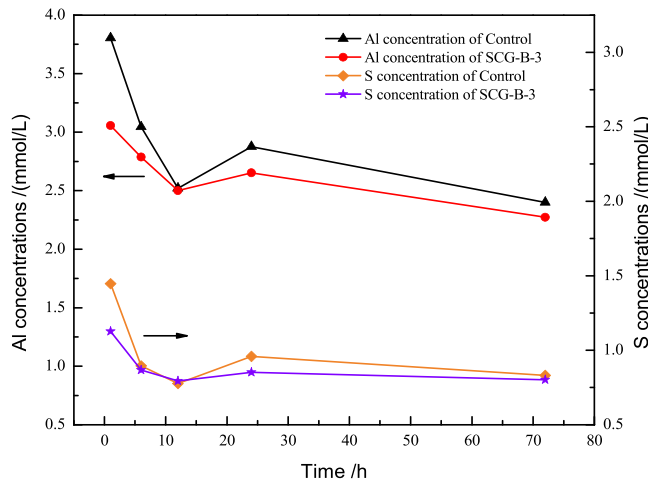


Fig. 14. Ion concentration of Al and S in the control and SCG-B-3 cement solution.

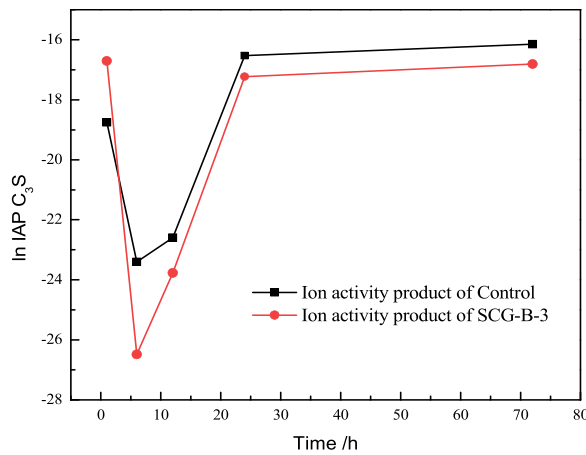


Fig. 15. ln IAP of C₃S in Control and SCG-B-3 cement composite.

large amount of Si was consumed in the early hydration age, the reaction rate of Si and the precipitation formation rate in the cement slowed down, the rate of Si consumption was decreased, the results were similar to those of the change of the Ca concentration. However, as the nucleation site effect of the GO, the hydration rate of CS in the SCG composites was accelerated, the supplementing rate of Si to the solution was faster, and Si concentration in the SCG was higher than the control from 12 h. The results also proved that SCG could effectively promote the dissolution of CS and accelerate cement hydration. Compared with the control specimen, the Si concentration increased by 15.3 % at 72 h in SCG-B composite.

The concentration variation diagrams of Al and S elements in the cement solutions is shown in Fig. 14. The existing forms of Al element are AlO_2^- or $\text{Al}(\text{OH})_4^-$ in cement solution, the existing form of S element is SO_4^{2-} , derived from gypsum in cement. During the hydration process, the concentration of Al element (C_{Al}) in the control cement solution was higher than that of the SCG composites. Under the promoting effect of SCG, ettringite was rapidly generated and precipitated on the surface of C_3A , accelerating the consumption of Al element. At the same time, the dissolution rate of C_3A was also reduced. In particular, the C_{Al} of the control and the SCG both increased between 12 h to 24 h, the generation rate of ettringite decreased, and the dissolution of C_3A dominated, thus causing the increase in C_{Al} in cement solution.

For S element, it can be seen from Fig. 14 that the change trend is the same as that of Al element. After the incorporation of SCG, compared with the control, the consumption of gypsum in SCG group within 1 h increased by 22.2 %. During the period of 12 h to 24 h, the concentration of element S (C_{S}) increased due to the dissolution of gypsum. The C_{S} in SCG composites was lower than the control in the hydration period, which showed that the incorporation of SCG had a significant promoting effect on the consumption of gypsum and promoted the formation of ettringite in the early stage of hydration.

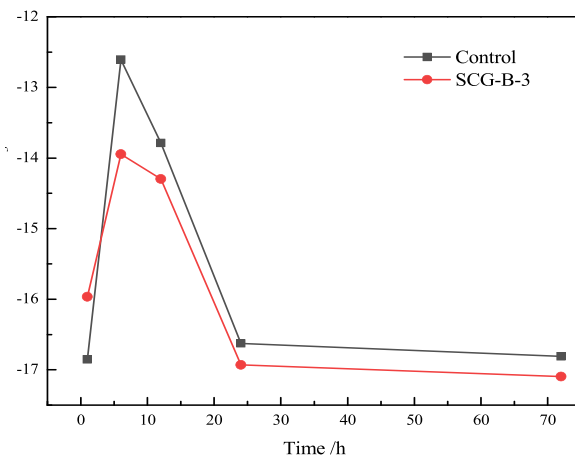


Fig. 16. Saturation index of C₃S in Control and SCG-B-3 cement composite.

3.8. Effect of SCG on the thermodynamic parameter of the cement

Based on the test results of ICP-AES, thermodynamic calculations were conducted to obtain the ion concentration of C₃S in the cement solution, as shown in Fig. 15. When water to cement ratio (w/s) was 0.35, the ln IAP of C₃S in the control was between -24 and -16, while that of the SCG composites was between -27 and -16. This is similar to the research results of Naber [46,47], whose study pointed out that when the w/s was 0.5, the ln IAP of C₃S was between -41 and -43. In the report of Nicoleau [48], it was pointed out that under the conditions of w/s = 5000 and w/s = 10000, the ln IAP range of C₃S was between -96 and -81. This also indicates that the results in this paper are reasonable, because a higher water to cement ratio would provide a greater dissolution driving force.

From the change in the ion activity product of C₃S, it can be seen that within 1–6 h, the absolute values of the ion activity product of C₃S in both groups showed an upward trend. This may be due to the faster hydration rate of C₃S in the early stage, and the rapid generation of hydration products resulting in an increase in the unsaturation of C₃S in the solution. After 6 h of hydration, the generation rate of hydration products decreased, and the unsaturation of C₃S began to decrease slowly. It can be seen that in the SCG-B composites, the ln IAP of C₃S was always lower than the control, which showed a higher unsaturation of C₃S than that of the control, it can be proved that the incorporation of SCG particles could significantly promote the dissolution of C₃S.

The saturation index (SI) of C₃S in the composite cement system is shown in Fig. 16, the saturation index of C₃S in the control is less than that in the SCG before 1 h, which showed that the degree of unsaturation of C₃S in the control is greater than that in the SCG group before 1 h. However, from 1 h to 3 d, the degree of unsaturation of C₃S in the SCG-B composites is greater than that in the control, which indicated that SCG-B provided a greater dissolution driving force for C₃S, promoted the continuous dissolution of C₃S and the generation of more C-S-H gel.

3.9. XPS analysis

XPS spectra of control and SCG-B-3 specimens are shown in Fig. 17 and Fig. 18, it can be seen that as the incorporating of SCG, the narrow peaks of Ca2p and Si2p both become higher, the binding energy of Ca2p and Si2p were also improved at 1 h and 3 d, the result showed that more compact C-S-H gel was formed in the SCG composites, the incorporation of SCG could more effectively promote the cement hydration, inducing the generation of highly polymerized C-S-H gel [49].

3.10. TEM-EDS analysis

TEM images and EDS energy spectra of C-S-H in the SCG-B-3 specimen is shown in Fig. 19, respectively. It can be seen from Fig. 19(a) that at 3 d of hydration, most of the generated C-S-H gels are filamentous and foil-like, with a low stacking density and a relatively sparse structure. However, obvious needle-like and granular at the edges can be observed at 28 d, as seen in Fig. 19(b), more obvious stacking shadows can also be seen. It can also be seen from the EDS spectra that the distribution of C-S-H is more dense at 28 d, and the formed C-S-H has a Ca/Si of 2.48, which is higher than 2.35 at 3 d, indicating that a large amount of C-S-H gels has been formed, and the C-S-H gels stack on each other to form a dense microstructure.

4. Conclusion

Nano-SiO₂ and CaCO₃ were used as supporting materials of GO (graphene oxide) and the SiO₂-CaCO₃-GO was prepared, the self-repairing performance of the SiO₂-CaCO₃-GO were characterized and the thermodynamic study on the cement hydration behavior was studied, the main conclusions are as follows.

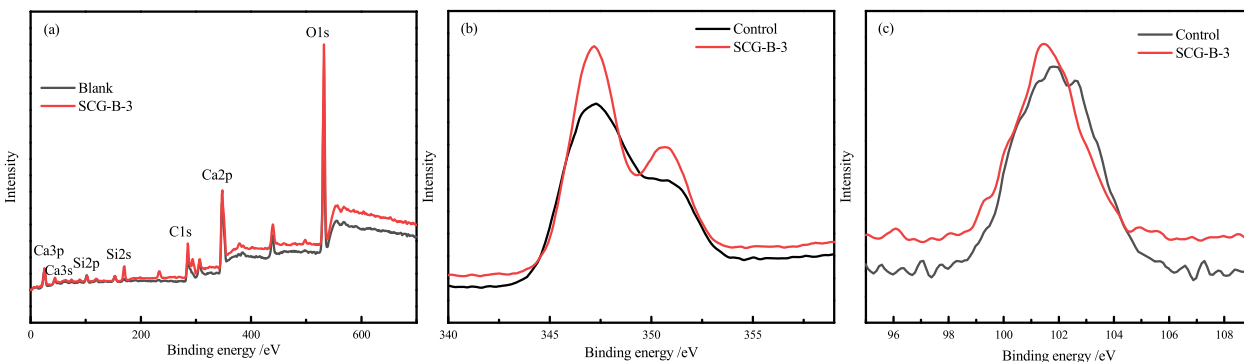


Fig. 17. XPS spectroscopy of control and SCG-B-3 specimen at 1 h: (a) wide range; (b) Ca2p; (c) Si2p.

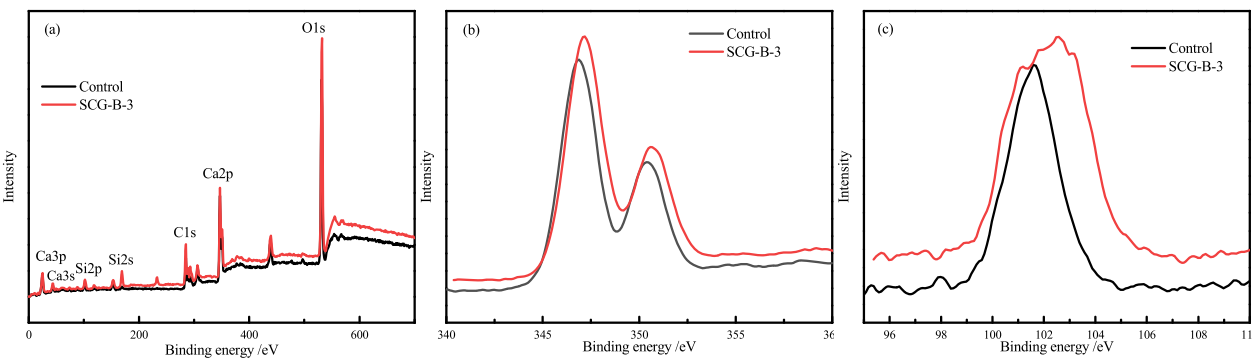


Fig. 18. XPS spectroscopy of control and SCG-B-3 specimen at 3 d: (a) wide range; (b) Ca2p; (c) Si2p.

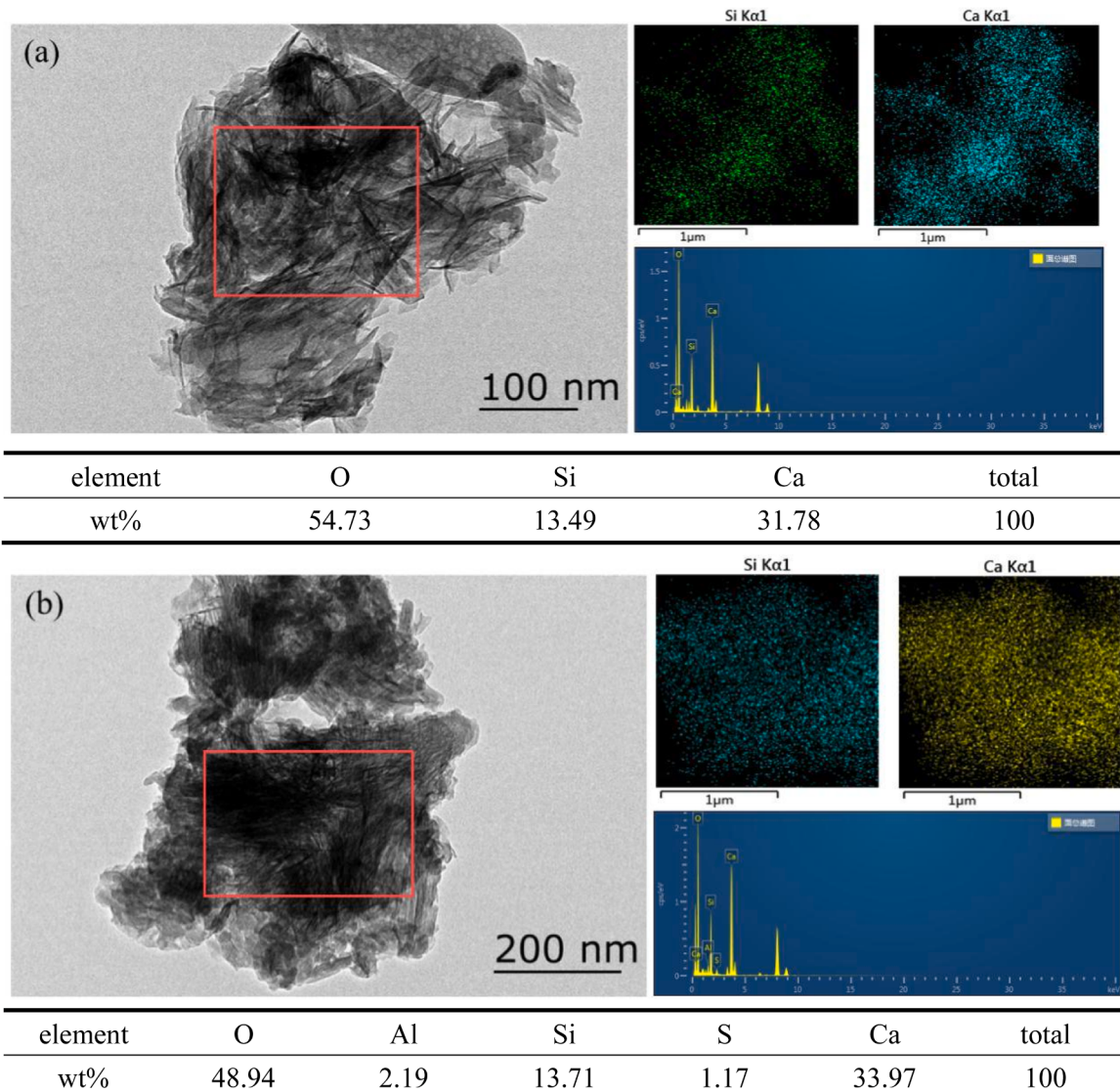


Fig. 19. TEM-EDS images of SCG-B-3 cement composite: (a) 3 d; (b) 28 d.

- (1) With the improved content of GO in SCG, the self-repairing performance of cement composites was further improved, the compressive strength repair rate with SCG reached 7.4 % after 7 d post-repairing and the surface crack repair rate reached 100 % at 28 d.
- (2) The incorporation of SCG promoted the consumption of $\text{Ca}(\text{OH})_2$, thereby increasing the degree of cement hydration. The more content of GO in SCG enable a better nucleation site effect, the interface between the cement matrix and the SCG gradually disappeared and filled by the hydration products.
- (3) The unsaturation of C_3S was improved as the addition of SCG, which provided a greater dissolution driving force for calcium silicate minerals $\text{CS}(\text{C}_2\text{S}/\text{C}_3\text{S})$ in cement, induced the generation of highly polymerized structure of C-S-H gel.

CRediT authorship contribution statement

Hu Dexin: Writing – original draft, Visualization, Software, Methodology, Investigation. **Wang Hailiang:** Visualization, Validation, Methodology. **Cai Lei:** Validation, Investigation, Data curation. **Deng Xiangong:** Validation, Supervision, Software, Project administration. **Niu Chen:** Validation, Investigation, Data curation. **Li Dongxu:** Supervision, Resources, Funding acquisition. **Zhang Yi:** Writing – review & editing, Writing – original draft, Validation, Supervision, Formal analysis, Data curation, Conceptualization.

Declaration of Competing Interest

The authors declare that they have no known competing financial interests or personal relationships that could have appeared to influence the work reported in this paper.

Acknowledgements

The financial support from the National Natural Science Foundation of China (No. 51872137) is gratefully acknowledged.

Data availability

Data will be made available on request.

References

- [1] L. Wang, H.Q. Yang, S.H. Zhou, E. Chen, S.W. Tang, Mechanical properties, long-term hydration heat, shrinkage behavior and crack resistance of dam concrete designed with low heat Portland (LHP) cement and fly ash, *Constr. Build. Mater.* 187 (2018) 1073–1091.
- [2] X. Wu, H. Huang, H. Liu, J. Hu, J. Wei, Z. Jiang, G. Ye, Q. Yu, B. Lothenbach, Reactions of self-healing agents and the chemical binding of aggressive ions in sea water: Thermodynamics and kinetics, *Cem. Concr. Res.* 145 (2021).
- [3] M. Tafesse, A. Shiferaw Alemu, B. Yang, S. Park, H.-K. Kim, Crack monitoring strategy for concrete structures in various service conditions via multiple CNT-CF/cement composite sensors: Experiment and simulation approaches, *Cem. Concr. Compos.* 143 (2023).
- [4] E. Batuecas, F. Liendo, T. Tommasi, S. Bensaid, F.A. Deorsola, D. Fino, Recycling CO₂ from flue gas for CaCO₃ nanoparticles production as cement filler: A Life Cycle Assessment, *J. J. CO₂. Util.* 45 (2021).
- [5] M. Wu, X. Hu, Q. Zhang, Y. Zhao, Y. Feng, H. Yuan, Synergistic effect of OH-rich fibers and mineral capsules on the self-healing properties of cement mortar, *Cem. Concr. Compos.* 137 (2023).
- [6] L. Wang, Z. Zhu, A. Hamza Ahmed, M. Liebscher, X. Zhu, V. Mechtkherine, Self-healing behavior of high-strength strain-hardening cement-based composites (HS-SHCC) blended with limestone calcined clay cement (LC3), *Constr. Build. Mater.* 370 (2023).
- [7] Y.-S. Wang, X.-Y. Wang, Effects of sodium carbonate on self-healing properties of cement–slag–limestone powder ternary cementitious material, *Case. Stud. Constr. Mater.* 17 (2022).
- [8] M. Wang, R. Wang, H. Yao, S. Farhan, S. Zheng, C. Du, Study on the three dimensional mechanism of graphene oxide nanosheets modified cement, *Constr. Build. Mater.* 126 (2016) 730–739.
- [9] L. Zhao, S. Zhu, H. Wu, X. Zhang, Q. Tao, L. Song, Y. Song, X. Guo, Deep research about the mechanisms of graphene oxide (GO) aggregation in alkaline cement pore solution, *Constr. Build. Mater.* 247 (2020).
- [10] E. Shamsaei, F.B. de Souza, X. Yao, E. Benhalal, A. Akbari, W. Duan, Graphene-based nanosheets for stronger and more durable concrete: A review, *Constr. Build. Mater.* 183 (2018) 642–660.
- [11] Q. Wang, S. Li, S. Pan, X. Cui, D.J. Corr, S.P. Shah, Effect of graphene oxide on the hydration and microstructure of fly ash-cement system, *Constr. Build. Mater.* 198 (2019) 106–119.
- [12] H. Yang, D. Hou, D. Zheng, L. Tang, W. Tang, H. Cui, Mechanical properties and mechanisms of alkali-activated slag paste reinforced by graphene oxide-SiO₂ composite, *Clean. Prod.* 378 (2022).
- [13] R. Yang, P. Zhang, T. Huang, D. Wang, Q. Sun, Z. Mao, S. Liu, Y. Li, W. Wang, Reinforcement effect and mechanism of graphene oxide on mortar with alkali free liquid accelerator, *Constr. Build. Mater.* 440 (2024).
- [14] L. Zhao, X. Guo, C. Ge, Q. Li, L. Guo, X. Shu, J. Liu, Investigation of the effectiveness of PC@GO on the reinforcement for cement composites, *Constr. Build. Mater.* 113 (2016) 470–478.
- [15] H. Zeng, S. Qu, Y. Tian, Y. Hu, Y. Li, Recent progress on graphene oxide for next-generation concrete: Characterizations, applications and challenges, *J. Build. Eng.* 69 (2023).
- [16] H. Yang, H. Cui, W. Tang, Z. Li, N. Han, F. Xing, A critical review on research progress of graphene/cement based composites, *Compos. Appl. Sci. Manuf.* 102 (2017) 273–296.
- [17] G. Mishra, A. Warda, S.P. Shah, Carbon sequestration in graphene oxide modified cementitious system, *J. Build. Eng.* 62 (2022).
- [18] H. Peng, Y. Ge, C.S. Cai, Y. Zhang, Z. Liu, Mechanical properties and microstructure of graphene oxide cement-based composites, *Constr. Build. Mater.* 194 (2019) 102–109.
- [19] N.J. Edwards, Y. Lin, H. Du, D. Ruan, Effect of graphene oxide on cement mortar under quasi-static and dynamic loading, *J. Build. Eng.* 74 (2023).
- [20] B. Liu, L. Wang, G. Pan, D. Li, Dispersion of graphene oxide modified polycarboxylate superplasticizer in cement alkali solution for improving cement composites, *J. Build. Eng.* 57 (2022).
- [21] X. Li, L. Wang, Y. Liu, W. Li, B. Dong, W.H. Duan, Dispersion of graphene oxide agglomerates in cement paste and its effects on electrical resistivity and flexural strength, *Cem. Concr. Compos.* 92 (2018) 145–154.
- [22] S.C. Devi, R.A. Khan, Effect of graphene oxide on mechanical and durability performance of concrete, *J. Build. Eng.* 27 (2020).
- [23] H.D. Nguyen, Q. Zhang, K. Sagoe-Crentsil, W. Duan, Graphene oxide-coated sand for improving performance of cement composites, *Cem. Concr. Compos.* 124 (2021).
- [24] Z. Lu, A. Hanif, C. Ning, H. Shao, R. Yin, Z. Li, Steric stabilization of graphene oxide in alkaline cementitious solutions: Mechanical enhancement of cement composite, *Mater. Des.* 127 (2017) 154–161.
- [25] Z. Lu, B. Chen, C.Y. Leung, Z. Li, G. Sun, Aggregation size effect of graphene oxide on its reinforcing efficiency to cement-based materials, *Cem. Concr. Compos.* 100 (2019) 85–91.
- [26] C. Luan, Y. Zhou, Y. Liu, Z. Ren, J. Wang, L. Yuan, S. Du, Z. Zhou, Y. Huang, Effects of nano-SiO₂, nano-CaCO₃ and nano-TiO₂ on properties and microstructure of the high content calcium silicate phase cement (HCSC), *Constr. Build. Mater.* 314 (2022).
- [27] S. Bai, X. Guan, G. Li, Effect of the early-age frost damage and nano-SiO₂ modification on the properties of Portland cement paste, *Constr. Build. Mater.* 262 (2020).
- [28] Q. Chen, K. Xie, G. Tao, S. Nimbalkar, P. Peng, H. Rong, Laboratory investigation of microstructure, strength and durability of cemented soil with Nano-SiO₂ and basalt fibers in freshwater and seawater environments, *Constr. Build. Mater.* 392 (2023).
- [29] W. Li, F.U.A. Shaikh, L. Wang, Y. Lu, B. Wang, C. Jiang, Y. Su, Experimental study on shear property and rheological characteristic of superfine cement grouts with nano-SiO₂ addition, *Constr. Build. Mater.* 228 (2019).
- [30] T. Zhang, Z. Wang, W. Wang, G. Li, H. Guo, H. Zhang, Property enhancement and mechanism of cement-based composites from the perspective of nano-silica dispersion improvement, *Case Stud. Constr. Mater.* 22 (2025).
- [31] A.M. Yassin, M.M. Eldin, M.S. Omar, M.A. Hafez, M.A. Elnagggar, Effect of nano-silica on the flexural behavior and mechanical properties of self-compacted high-performance concrete (SCHPC) produced by cement CEM II/A-P (experimental and numerical study), *Case Stud. Constr. Mater.* 21 (2024).

- [32] C. Huang, T. Nantung, Y. Feng, N. Lu, Effect of colloidal nano silica on the freeze-thaw resistance and air void system of portland cement concrete, *J. Build. Eng.* 86 (2024).
- [33] J. Xia, W. Zhang, Y. Du, J. Wang, J. Wang, L. Ren, J. Zhao, M. Yang, H. Li, F. Leng, Cooperative stabilization of calcium carbonate powder, blast furnace slag, and white cement in composite concrete: Volume variation and hydration behavior, *Constr. Build. Mater.* 450 (2024).
- [34] P. Saingam, B. Chatveera, P. Promsawat, Q. Hussain, A. Nawaz, N. Makul, G. Sua-iam, Synergizing Portland Cement, high-volume fly ash and calcined calcium carbonate in producing self-compacting concrete: A comprehensive investigation of rheological, mechanical, and microstructural properties, *Case Stud. Constr. Mater.* 21 (2024).
- [35] T. Meng, Y. Qiang, A. Hu, C. Xu, L. Lin, Effect of compound nano-CaCO₃ addition on strength development and microstructure of cement-stabilized soil in the marine environment, *Constr. Build. Mater.* 151 (2017) 775–781.
- [36] K. Cui, D. Lau, Y. Zhang, J. Chang, Mechanical properties and mechanism of nano-CaCO₃ enhanced sulfoaluminate cement-based reactive powder concrete, *Constr. Build. Mater.* 309 (2021).
- [37] B. Aytekin, A. Mardani, S. Yazici, State-of-art review of bacteria-based self-healing concrete: Biominerilization process, crack healing, and mechanical properties, *Constr. Build. Mater.* 378 (2023).
- [38] L. Li, T. Liu, G. Jiang, C. Fang, B. Qu, S. Zheng, G. Yang, C. Tang, Insight into the temperature stimulation on the self-healing properties of cement-based materials, *Constr. Build. Mater.* 361 (2022).
- [39] X. Du, Z. Si, D. Qi, Y. Li, L. Huang, Y. Zhang, Y. Gao, Optimization of spore production and activation conditions of concrete crack healing bacteria and research on crack repair effect, *Constr. Build. Mater.* 394 (2023).
- [40] C. Fu, Q. Zhan, X. Zhang, J. Zhou, Y. Wu, X. Li, P. Zhou, G. Xu, Self-healing properties of cement-based materials in different matrix based on microbial mineralization coupled with bimetallic hydroxide, *Constr. Build. Mater.* 400 (2023).
- [41] K. Yin, Z. Luo, X. Liu, H. Pan, T. Zhi, H. Feng, Y. Song, Y. Su, Preparation and application of Na₂SiO₃@EC microcapsules for self-healing alkali-activated slag, *Constr. Build. Mater.* 400 (2023).
- [42] P. Azarsa, R. Gupta, A. Biparva, Assessment of self-healing and durability parameters of concretes incorporating crystalline admixtures and Portland Limestone Cement, *Cem. Concr. Compos.* 99 (2019) 17–31.
- [43] Q. Ren, Q. Wang, Z. Wu, J. Liu, H.-Q. Xu, A. Wang, X. Zhang, Z. Zhang, Y. Ding, Research on the properties of crystalline admixtures: Self-healing healing materials for concrete from multiple perspectives, *Constr. Build. Mater.* 453 (2024).
- [44] X. Kang, X. Zhu, J. Liu, X. Shu, Y. Huang, J. Qian, Dissolution and precipitation behaviours of graphene oxide / tricalcium silicate composites, *Compos. B Eng.* 186 (2020).
- [45] J.W. Bullard, G.W. Scherer, An Ideal Solid Solution Model for C-S-H, *J. Am. Ceram. Soc.* 99 (12) (2016) 4137–4145.
- [46] C. Naber, F. Bellmann, J. Neubauer, Influence of w/s ratio on alite dissolution and C-S-H precipitation rates during hydration, *Cem. Concr. Res.* 134 (2020).
- [47] C. Naber, F. Bellmann, T. Sowoidnich, F. Goetz-Neunhoeffer, J. Neubauer, Alite dissolution and C-S-H precipitation rates during hydration, *Cem. Concr. Res.* 115 (2019) 283–293.
- [48] L. Nicoleau, A. Nonat, D. Perrey, The di- and tricalcium silicate dissolutions, *Cem. Concr. Res.* 47 (2013) 14–30.
- [49] K. Kurumisawa, T. Nawa, H. Owada, M. Shibata, Deteriorated hardened cement paste structure analyzed by XPS and ²⁹Si NMR techniques, *Cem. Concr. Res.* 52 (2013) 190–195.